Analytical and Bioanalytical Chemistry
https://doi.org/10.1007/s00216-020-02552-5

RESEARCH PAPER

Highly sensitive electrochemiluminescence biosensor for $VEGF_{165}$ detection based on a g-C_3N_4/PDDA/CdSe nanocomposite

Jin-long Cheng[1] · Xing-Pei Liu[1] · Jing-Shuai Chen[1] · Chang-jie Mao[1] · Bao-Kang Jin[1]

Received: 4 November 2019 / Revised: 14 February 2020 / Accepted: 26 February 2020

Abstract

In this work, an electrochemiluminescence (ECL) biosensor was fabricated for the selective detection of vascular endothelial growth factor ($VEGF_{165}$). g-C_3N_4/PDDA/CdSe nanocomposites were used as the ECL substrate. Then, DNA labeled at the 5′ end with amino groups (DNA_1) was immobilized on the surface of g-C_3N_4/PDDA/CdSe nanocomposite-modified glassy carbon electrode (GCE) by amido linkage. AuNP-labeled target DNA (Au-DNA_2) could hybridize with DNA_1 to form a double strand. The ECL of the g-C_3N_4/PDDA/CdSe nanocomposite was efficiently quenched due to the resonance energy transfer between CdSe QDs and Au NPs. After $VEGF_{165}$ was recognized and bound by Au-DNA_2, the double helix was disrupted, and the energy transfer was broken. In this case, Au-DNA_2 was released from the electrode surface, and the ECL intensity recovered to a higher level. Under optimal conditions, this ECL biosensor possesses excellent selectivity, accuracy, and stability for $VEGF_{165}$ detection in a linear range of 2 pg mL^{-1} to 2 ng mL^{-1} with a detection limit of 0.68 pg mL^{-1}. In addition, this assay has been successfully applied to the determination of $VEGF_{165}$ in serum samples.

Keywords Electrochemiluminescence (ECL) · g-C_3N_4/PDDA/CdSe · DNA · Vascular endothelial growth factor ($VEGF_{165}$)

Introduction

Vascular endothelial growth factor $(VEGF)_{165}$ is a significant signaling protein involved in vasculogenesis [1]. This protein plays an important role in the supervision of vascular permeabilization and angiogenesis [1]; thus, it can be used as a serum biomarker of human diseases, such as Parkinson's disease, rheumatoid arthritis [2], brain injuries [3], psoriasis [4], and cancer [5–7]. In addition, $VEGF_{165}$ can also be applied to restore oxygen to tissues when blood circulation is inadequate [8]. However, compared with the $VEGF_{165}$ level in healthy people ($VEGF_{165}$ concentration of 2.30–467.10 pg mL^{-1}) [9], $VEGF_{165}$ overexpression may indicate vascular diseases, such as bronchial asthma [18], mellitus diabetes [10], and damage to the retina of the eye and other parts of the body [11–13]. These diseases all lead to overexpression of $VEGF_{165}$. In contrast, patients who have a disease relating to a neurological disorder are observed to exhibit low expression of $VEGF_{165}$. Accordingly, treatment is proposed to increase the $VEGF_{165}$ level to inhibit neuron degeneration [14]. Thus, a rapid, sensitive, and selective method for $VEGF_{165}$ detection is urgently needed for disease diagnosis and the supervision of subsequent treatment.

The application of aptamer DNA in biosensors as a powerful molecular recognition element has attracted increasing attention. Aptamer DNA is an artificial nucleic acid that has high specificity and affinity against its target [15–21]. In contrast to antibodies, aptamer DNA has a number of distinctive advantages, such as being chemically stable and small in size and having high selectivity, high stability, high sensitivity in harsh biological environments; easy synthesis procedures; and low production costs. To date, the detection of $VEGF_{165}$ based on aptamer strategies has involved various signal transduction methods, including electrochemiluminescence (ECL), ELISA [22], immunohistochemistry fluorescence spectrometry [23], and optical and electrochemical techniques [24–26]. However, these methods are labor-intensive and time-consuming and often require intricate apparatuses, which limits their widespread use. In contrast, ECL has unique

✉ Chang-jie Mao
maochangjie@sina.com

[1] Key Laboratory of Structure and Functional Regulation of Hybrid Materials (Ministry of Education), Anhui Province Key Laboratory of Chemistry for Inorganic/Organic Hybrid Functionalized Materials, School of Chemistry & Chemical Engineering, Anhui University, Hefei 230601, Anhui, China

Published online: 11 March 2020

advantages, such as rapidity, low background, low cost, simplicity, and high sensitivity [27]. Therefore, in this work, we construct a convenient and sensitive ECL method based on target recognition by a DNA aptamer for the detection of $VEGF_{165}$.

Graphite-like carbon nitride (g-C_3N_4), which is the most stable carbon nitride allotrope, has drawn significant attention because of its hypotoxicity, biocompatibility, chemical stability, outstanding photoactivity, photocatalytic properties, high chemical stability [28, 29], and small band gap (2.69 eV) [30]. Due to these advantages, g-C_3N_4 is used in several applications, such as photoelectrochemistry, chemical sensing, and catalysis. Nevertheless, the application of g-C_3N_4 has been somewhat limited due to its chemical inertia and high recombination rate of photogenerated electron-hole pairs [28, 29]. Thus, g-C_3N_4 should be modified to overcome these drawbacks and extend its potential applications. Recently, CdSe quantum dots (QDs) have attracted great research interest because of their high quantum yield, electrochemical properties, and unique size dependence. Simultaneously, the energy levels of CdSe QDs can match the band gap of g-C_3N_4, which effectively extends their light-capturing ability and restrains the recombination of photogenerated electron-hole pairs [30, 35]. Because of these properties, the ECL intensity of g-C_3N_4/CdSe is greatly increased. However, its stability has not yet been improved, because CdSe QDs and g-C_3N_4 are negatively charged. Polydiallyldimethylammonium chloride (PDDA) could act as a binder due to its positive charge [42]. CdSe/PDDA/g-C_3N_4 nanocomposites have not only high ECL strength but also good ECL stability.

A convenient ECL biosensor to detect $VEGF_{165}$ based on g-C_3N_4/PDDA/CdSe nanocomposites was constructed [43]. Scheme 1 describes the steps of the ECL biosensor fabrication. First, the g-C_3N_4/PDDA/CdSe composite was added to a prepared glassy carbon electrode (GCE) and dried in air. Then, DNA_1 was incubated on the modified electrode overnight. Finally, Au-DNA_2 was dropped on the electrode to form the biosensor. Then, the constructed biosensor electrode was applied for the detection of $VEGF_{165}$. The prepared ECL biosensor could offer a stable, specific, and novel strategy for the detection of other biomolecules.

Experimental section

Materials and reagents

Selenium, cadmium chloride ($CdCl_2$), melamine, and L-cysteine were purchased from Aladdin Reagent Co., Ltd. (Shanghai, China). Chloroauric acid ($HAuCl_4{\cdot}4H_2O$), potassium chloride (KCl, 99.5%), potassium hexacyanoferrate trihydrate ($K_4[Fe(CN)_6]{\cdot}3H_2O$, 99.5%), disodium hydrogen phosphate dodecahydrate ($Na_2HPO_4{\cdot}12H_2O$, 99%), poly(diallyldimethylammonium chloride) (PDDA, Mw 200,000–350,000, 20 wt% in H_2O), N-hydroxysuccinimide (NHS), and ethyl-(3-methyl-propyl)carbodiimide amine hydrochloride (EDC) were acquired from Sinopharm Chemical Reagent Co., Ltd. (Shanghai, China). Sodium chloride (NaCl, 99.5%), peroxodisulfate ($K_2S_2O_8$, 99.5%), potassium phosphate monobasic (KH_2PO_4, 99%), and sodium sulfite anhydrous (Na_2SO_3) were purchased from Guangfu Chemical Reagent Co., Ltd. (Tianjin, China).

DNA_1 (5′-NH_2-TTTTTTTTTTTTGGCCAGCACACCCACC-3′), aptamer DNA_2 ($VEGF_{165}$, 5′-SH-GGCCCGTATGGTGGGTGTGCTGGCC-3′), 1× TE buffer, interleukin-6 (IL-6), urokinase-type plasminogen activator (u-PA), mucin 1 (MUC1), and the target $VEGF_{165}$ were purchased from Shanghai Sangon Biological Engineering Technology Co., Ltd. (Shanghai, China).

Human serum samples were provided by The First Affiliated Hospital of Anhui Medical University.

Instrumentation

Ultraviolet-visible (UV-vis) absorption spectra were recorded on a UV-3600 UV spectrometer (Shimadzu Ltd., Japan). Transmission electron microscopy (TEM) images were carried out with a JEM-2100 transmission electron microscope (JEOL Ltd., Japan). The photoelectrochemical measurements were performed on a CHI 660E electrochemical workstation (CH Instruments, China) with a traditional three electrode system consisting of a modified GCE as the working electrode, a Pt electrode as the counter electrode, and Ag/AgCl (saturated KCl) as the reference electrode. EIS was performed on a Thales electrochemical workstation (ZAHNER-elektrik GmbH & Co, Germany) with a three electrode system consisting of a platinum electrode, a calomel electrode, and the modified GCE. The ECL emissions were obtained using an RFL-1 multifunctional electrochemical analytical system (Xi'an Remax Electronic Science & Technology Co., Ltd., Xi'an, China) with a three electrode system. The working potential was from 0 to − 1.45 V and the voltage of the photomultiplier tube was set as 400 V.

Synthesis of g-C_3N_4

The synthetic procedures of g-C_3N_4 were carried out according to previously reported method with slight modifications [31, 32]. The obtained bulk g-C_3N_4 was then dispersed into ultrapure water and ultrasonicated for 12 h. Finally, g-C_3N_4 nanosheets were obtained by centrifuging the prepared suspension at 10000 rpm for 15 min and then removing the moisture in a vacuum oven.

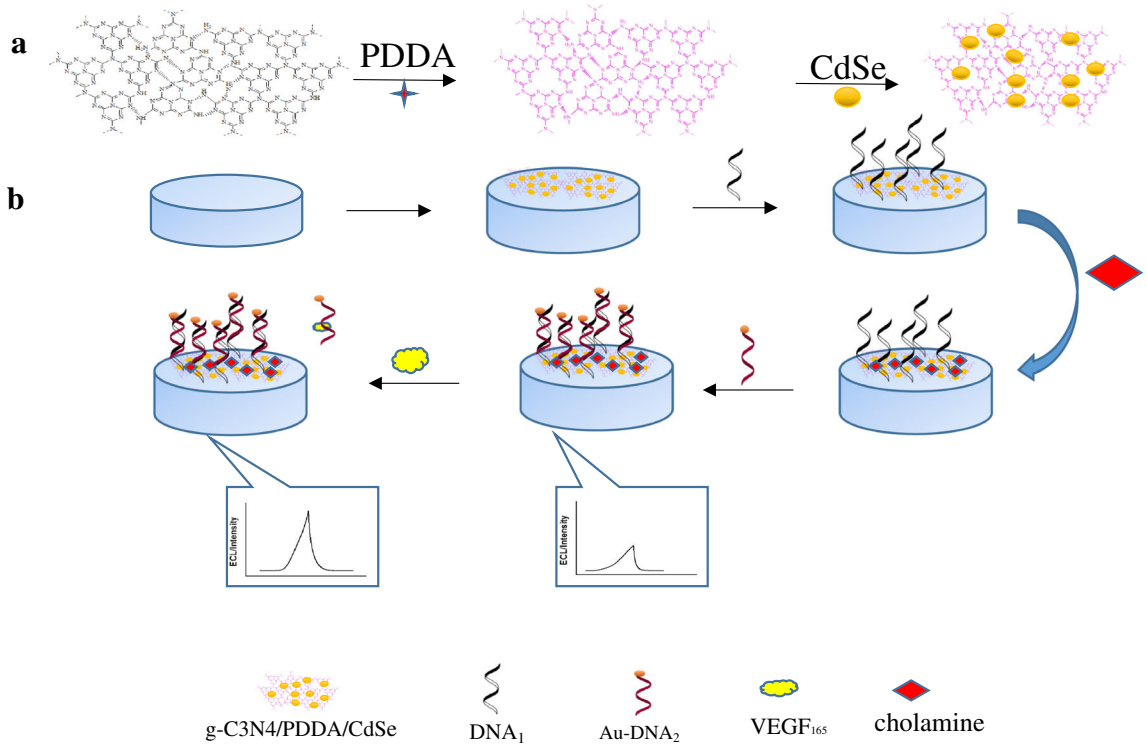

Scheme 1 Schematic diagram of entire electrochemiluminescence (ECL) sensor manufacturing and detection process

Synthesis of AuNPs and AuNP-labeled DNA_2

The AuNPs were synthesized based on the previously published method [33]. Twenty milliliters of $HAuCl_4$ (250 μmol mL^{-1}) and 600 μL of ice-cold $NaBH_4$ (0.1 mol mL^{-1}) were added to the beaker and stirred in an ice bath for 15 min. Finally, the reaction was stirred for another 3 h at room temperature. The obtained AuNPs were stored at 4 °C before use.

The AuNP-labeled DNA_2 were synthesized based on the method announced previously [33]. Ten microliters of TCEP (10 mM) was added to 200 μL of DNA_2 (5 μM) solution to break the S–S bonds of DNA_2. Next, 800 μL of purified colloid AuNPs was added to the solution. The solution was shaken for 16 h to ensure the formation of Au–S bonds. Finally, the solution was purified by centrifugation and redispersed in TE buffer. The acquired Au-DNA_2 solution was stored at 4 °C until use.

Synthesis of CdSe and g-C_3N_4/PDDA/CdSe composite

The L-cysteine-modified CdSe QDs were prepared according to the literature method [34]. The g-C_3N_4/PDDA/CdSe composite was synthesized as described in the previous literature with a slight modification [35]. The g-C_3N_4/PDDA was prepared by sonication. First, 100 mL of PDDA (0.2%) was added to the g-C_3N_4 suspension, and the mixture was sonicated for another 2 h and centrifuged. The precipitate was washed at least three times to remove excess PDDA. Finally, the solution was stored at 4 °C. Subsequently, 100 μL of CdSe was added to the 800 μL of the g-C_3N_4/PDDA suspension and sonicated for 240 min. Then, the g-C_3N_4/PDDA/CdSe composite was stored at 4 °C until use.

Construction of the ECL biosensor for determining $VEGF_{165}$

Scheme 1 describes the construction of the ECL biosensor [43]. First, 10 μL of g-C_3N_4/PDDA/CdSe nanocomposite was dropped on the cleaned GCE and dried. Next, the modified electrode was incubated with 20 μL of EDC/NHS (2:1) to activate the carboxylic acid groups and washed with TE buffer. Then, DNA_1 was dropped onto the GCE and incubated overnight. Next, 20 μL of cholamine was dropped onto the electrode and incubated for 1 h to cover the carboxylic acid groups. After that, Au-DNA_2 was dropped on the electrode and incubated for 2 h at 37 °C. Finally, the modified electrode was incubated with 20 μL of different concentrations of $VEGF_{165}$ and washed with TE buffer, and the prepared GCE was detected by an ECL analyzer.

The ECL value was obtained in 0.1 mol mL^{-1} PBS containing 0.1 mol mL^{-1} $K_2S_2O_8$ and 0.1 mol mL^{-1} KCl. The potential window was from 0 to − 1.45 V with a scan rate of 100 mV s^{-1}. The ECL intensity was then applied to analyze the relationship between the different concentrations of $VEGF_{165}$ and ECL intensity.

Results and discussion

Characterization of the materials

The morphologies of g-C_3N_4 and g-C_3N_4/PDDA/CdSe were characterized by high-resolution transmission electron microscopy (HR-TEM). As shown in Fig. 1 A, g-C_3N_4 displayed smooth surface with ultrathin layers of a nanosheet structure. Figure 1 B shows that the CdSe QDs were tightly dispersed on the g-C_3N_4 nanosheet surface. Figure 1 C displays the HR-TEM images of the g-C_3N_4/PDDA/CdSe nanocomposites. The lattice fringe of CdSe is clearly visible in the image. Thus, the TEM images show that CdSe QDs were tightly coated on the smooth surface of g-C_3N_4.

UV-vis spectroscopy was also used to record the optical properties of the g-C_3N_4, g-C_3N_4/PDDA, CdSe, and g-C_3N_4/PDDA/CdSe nanocomposites. As shown in Fig. 1 D, the pure g-C_3N_4 and g-C_3N_4/PDDA nanocomposites had characteristic absorption peaks at 320 nm (curve a) and 325 nm (curve b), respectively. The positions of the absorption peaks were similar to those in previous reports [33]. The pure CdSe QDs displayed wide absorption below 500 nm and an obvious absorption peak at 448 nm (curve c). The g-C_3N_4/PDDA/CdSe nanocomposite exhibited the characteristic absorption peaks of both the g-C_3N_4/PDDA and CdSe nanoparticles. Simultaneously, XRD was used to investigate the crystal structures of the CdSe, g-C_3N_4, and g-C_3N_4/PDDA/CdSe nanocomposites. As shown in Fig. 1 E, curve a shows that pure g-C_3N_4 had diffraction peaks at 12.6° (100) and 28.2° (002) (Card No. 019-0191]). CdSe (Curve b) contains three crystal structures associated with (111), (220), and (311). Curve c for the g-C_3N_4/PDDA/CdSe nanocomposite has crystal structures associated with (100), (002), (111), and (220). However, the (311) structure for CdSe is not shown in the g-C_3N_4/PDDA/CdSe nanocomposite, possibly because of its very low diffraction peak. Therefore, the combination of

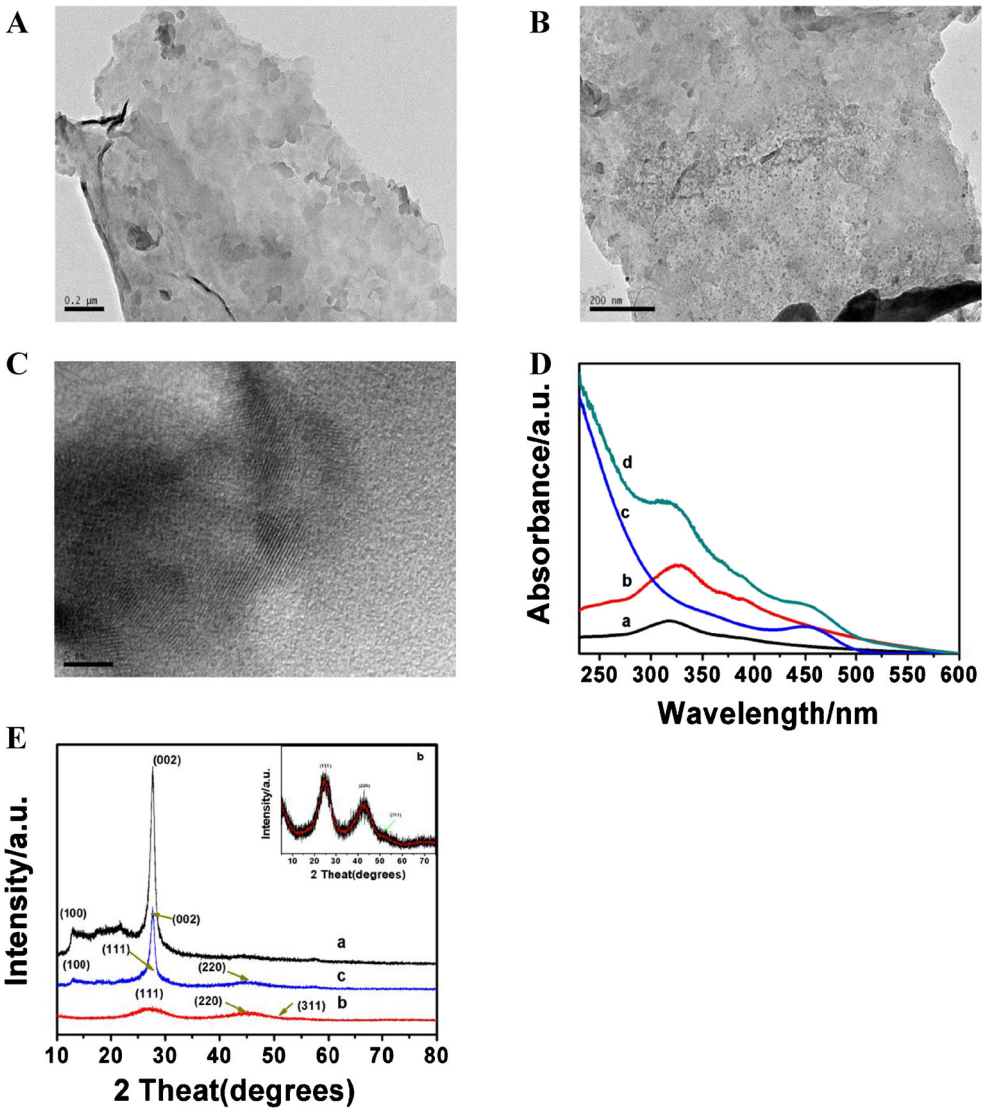

Fig. 1 (**A**) TEM image of g-C_3N_4. (**B**) TEM image of g-C_3N_4/PDDA/CdSe nanocomposite. (**C**) HR-TEM image of CdSe. (**D**) UV-vis of (**a**) g-C_3N_4, (**b**) g-C_3N_4/PDDA, (**c**) CdSe, and (**d**) g-C_3N_4/PDDA/CdSe nanocomposite. (**E**) XRD of (**a**) g-C_3N_4, (**b**) CdSe, and (**c**) g-C_3N_4/PDDA/CdSe nanocomposite

TEM image and UV-vis spectroscopy proves that the g-C_3N_4/PDDA/CdSe nanocomposite was synthesized successfully.

EIS and ECL behavior

To prove the advantage of the g-C_3N_4/PDDA/CdSe nanocomposite, the ECL intensity of pure g-C_3N_4 was acquired and compared with the ECL intensity of the g-C_3N_4/PDDA/CdSe nanocomposite. As presented in Fig. 2 A, the ECL results of g-C_3N_4 were quite unstable with low intensity. Figure 2 B presents the ECL intensity of the g-C_3N_4/PDDA/CdSe nanocomposite. The ECL results of g-C_3N_4 were clearly lower than those of the g-C_3N_4/PDDA/CdSe nanocomposite and showed high stability. Therefore, we used the g-C_3N_4/PDDA/CdSe nanocomposite as the ECL material. The probable mechanism of the ECL material is described as follows [35]:

$$g\text{–}C_3N_4/PDDA/CdSe + e^- \rightarrow g\text{–}C_3N_4/PDDA/CdSe^- \quad (1)$$

$$S_2O_8^{2-} + e^- \rightarrow SO_4^- \cdot + SO_4^{2-} \quad (2)$$

$$g\text{–}C_3N_4/PDDA/CdSe^{\cdot} + SO_4^{-\cdot} \rightarrow SO_4^{2-} + g\text{–}C_3N_4/PDDA/CdSe^* \quad (3)$$

$$g\text{–}C_3N_4/PDDA/CdSe^* \rightarrow g\text{–}C_3N_4/PDDA/CdSe + hv \quad (4)$$

EIS is a powerful tool for monitoring the fabrication process of the modified electrode step by step. It is well known that impedance spectra contain linear and semicircular parts, where the linear part represents the limited diffusion process at lower frequencies and the semicircular part is associated with the electron transfer limited process at higher frequencies. As shown in Fig. 2 C, the electric charge-transfer resistance (R_{ct}) value concerns the stepwise modification processes of the electrode. The bare electrode shows a small semicircular part, which represents the excellent conductivity of the bare electrode (curve a, R_{ct} value of 83.65 Ω). Curve b (R_{ct} value of 888.28 Ω) shows the impedance spectrum of the g-C_3N_4/PDDA/CdSe nanocomposite, where the semicircular part exhibits a large increase, meaning that the impedance is larger than that for the bare GEC. After the modified GCE was modified with DNA_1, the resistance increased again because the DNA sequences (curve c, R_{ct} value of 1147.26 Ω) had low conductivity. Subsequently, cholamine was covalently bound to the CdSe QDs to cover the remaining active sites. The R_{ct} increased (curve d, R_{ct} value of 1476.44 Ω) because cholamine reacted with the carboxyl groups of CdSe QDs and prevented the electron transfer of the electrode [36]. R_{ct} further increased (curve e, R_{ct} value of 1730.64 Ω) after Au-DNA_2 modification of the electrode. Therefore, the EIS results demonstrate that the ECL biosensor was fabricated successfully.

Simultaneously, the ECL intensity was obtained in 0.1 M PBS containing 0.1 M $K_2S_2O_8$, which was used to monitor the different fabrication steps of the ECL biosensor. As shown in Fig. 2 D, the electrode coated with g-C_3N_4/PDDA/CdSe showed the highest ECL intensity (Fig. 2D, curve a). After the GCE was modified with DNA_1 (Fig. 2D, curve b) and blocked by cholamine (Fig. 2D, curve c), the ECL intensity

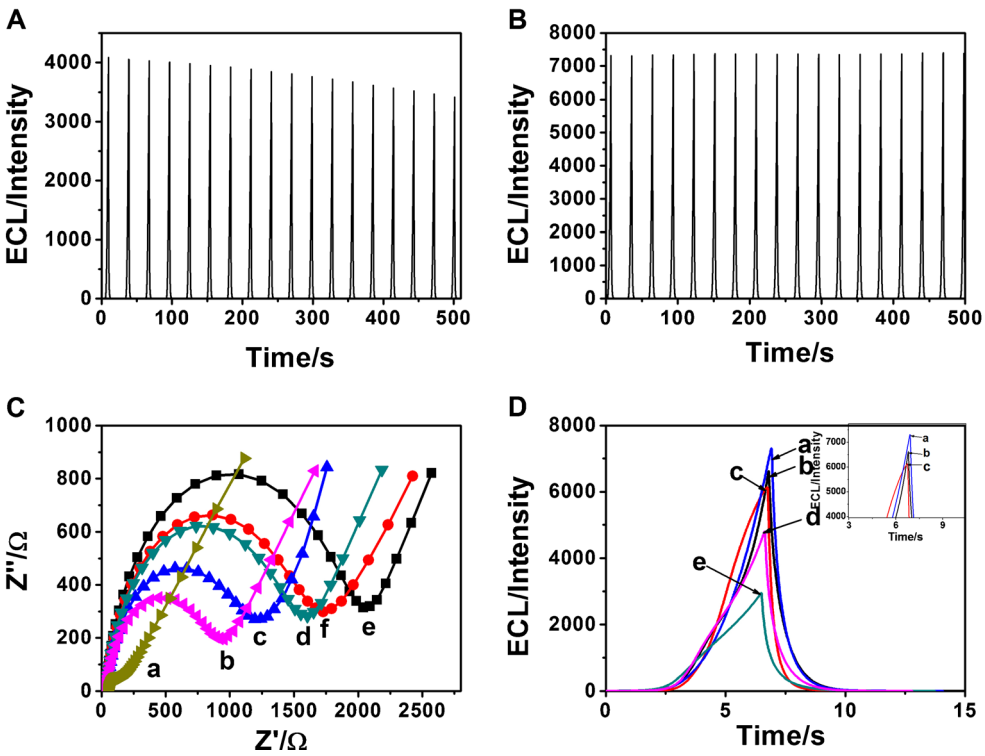

Fig. 2 ECL intensity of (**A**) g-C_3N_4 and (**B**) g-C_3N_4/PDDA/CdSe nanocomposite. (**C**) EIS of (**a**) bare GEC, (**b**) g-C_3N_4/PDDA/CdSe, (**c**) g-C_3N_4/PDDA/CdSe/DNA_1, (**d**) g-C_3N_4/PDDA/CdSe/DNA_1/cholamine, (**e**) g-C_3N_4/PDDA/CdSe/DNA_1/cholamine/Au-DNA_2, and (**f**) g-C_3N_4/PDDA/CdSe/DNA_1/cholamine/Au-DNA_2/$VEGF_{165}$. (**D**) ECL intensity of (**a**) g-C_3N_4/PDDA/CdSe, (**b**) g-C_3N_4/PDDA/CdSe/DNA_1, (**c**) g-C_3N_4/PDDA/CdSe/DNA_1/cholamine, (**d**) g-C_3N_4/PDDA/CdSe/DNA_1/cholamine/Au-DNA_2/$VEGF_{165}$, and (**e**) g-C_3N_4/PDDA/CdSe/DNA_1/cholamine/Au-DNA_2

decreased obviously because DNA_1 and cholamine covered the electrode and impeded electron transfer. Subsequently, the electrode was modified by dropping Au-DNA_2 on the electrode, and the ECL signals decreased to the lowest level (Fig. 2D, curve e). This result may be attributed to the low conductivity of Au-DNA_2 and the exciton energy transfer between CdSe QDs and Au NPs, which evidently prevented the photogenerated electrons in the conduction band of CdSe from transferring to the conduction band of g-C_3N_4. According to previous reports [33], the composite of Au-DNA_2 and g-C_3N_4/PDDA/CdSe exhibits appreciable spectral overlap; thus, efficient energy transfer can take place. After incubation with the target $VEGF_{165}$, the ECL signal increased distinctly (Fig. 2D, curve d), which means that Au-DNA_2 successfully combined with $VEGF_{165}$. Since the target $VEGF_{165}$ carried off part of the Au-DNA_2, its impedance decreased distinctly. The ECL results are in agreement with the impedance results, proving that the biosensor was constructed successfully. Thus, the results further demonstrate that the biosensor was successfully fabricated.

Optimization of the reaction conditions

To efficiently apply the prepared ECL biosensor to the detection of the target $VEGF_{165}$, it is vital to optimize the concentration of CdSe QDs because this concentration has an important influence on the ECL intensity. As presented in Fig. 3 A, the ECL signals increased with decreasing CdSe QD concentration. This result may be attributed to the blocking of electron transfer by excess CdSe QDs. When the ratio was 8:1 (g-C_3N_4/PDDA:CdSe), the ECL tended to exhibit steady results, and the results also showed the highest ECL intensity. When the ratio was lowered to 12:1 (g-C_3N_4/PDDA:CdSe), the ECL intensity decreased due to the small number of CdSe QDs on the surface of g-C_3N_4/PDDA. Hence, the concentration ratio of 8:1 was chosen for further use. The concentration of Au-DNA_2 is also a significant influencing factor. As presented in Fig. 3 B, the changes in the ECL intensity tended to be gentle when the concentration of Au-DNA_2 was up to 3 μM, meaning that DNA_1 could not combine with the excess of Au-DNA_2. The incubation times of Au-DNA_2 with DNA_1 and $VEGF_{165}$ with Au-DNA_2 also play a significant role in the entire detection process. As presented in Fig. 3 C, the ECL signals decreased with increasing incubation time and maintained a steady value after 45 min. The ECL intensity increased with increasing incubation time, and the ECL value tended to exhibit stable results after 60 min, as shown in Fig. 3 D. Hence, the optimal concentration of Au-DNA_2 was 3 μM. The best incubation times of Au-DNA_2 and $VEGF_{165}$ were 45 and 60 min, respectively.

Detection of target $VEGF_{165}$

With the optimal reaction conditions, the ECL intensity was investigated for different target concentrations. As presented in Fig. 4 A, the ECL signals of the constructed biosensor were clearly linearly dependent on the concentration of $VEGF_{165}$. The ECL value increased gradually with increasing $VEGF_{165}$

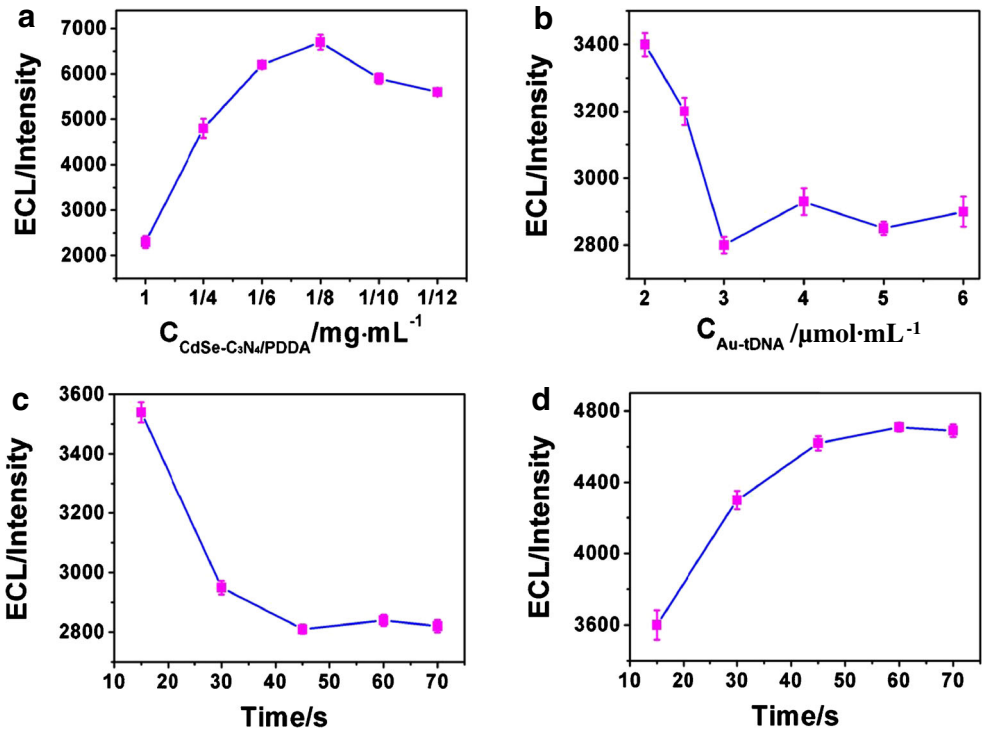

Fig. 3 Effects of (**A**) the concentration of CdSe-g-C_3N_4/PDDA nanocomposite, (**B**) the incubation time of DNA_1 with Au-DNA_2, (**C**) the concentration of $C_{Au\text{-}DNA_2}$, and (**D**) the incubation time of target $VEGF_{165}$

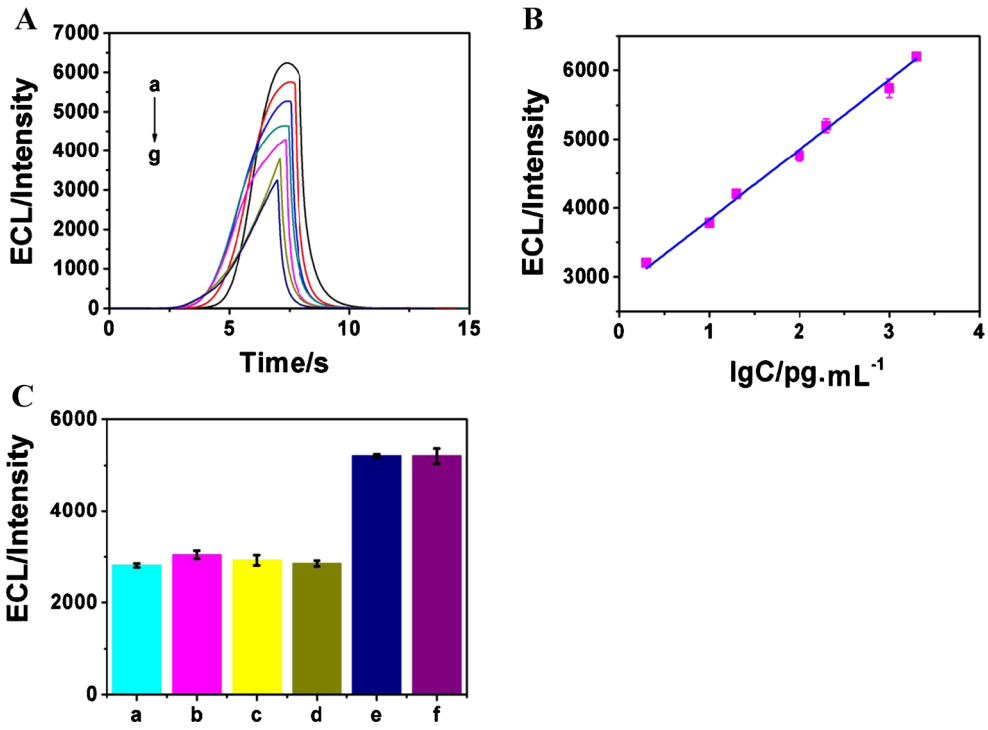

Fig. 4 (**A**) ECL intensity with the concentration of the target $VEGF_{165}$ of (**a**) 2, (**b**) 1, (**c**) 0.2, (**d**) 0.1, (**e**) 0.02, (**f**) 0.01, and (**g**) 0.002 ng ml. (**B**) Corresponding calibration curve of the biosensor for detecting the target $VEGF_{165}$. (**C**) Selectivity of constructed ECL biosensor with different targets: (**a**) blank. (**b**) 20 ng mL^{-1} of IL-6. (**c**) 20 ng mL^{-1} of u-PA. (**d**) 20 ng mL^{-1} of MUC1. (**e**) 0.2 ng mL^{-1} of $VEGF_{165}$. (**f**) a mixture containing 20 ng mL^{-1} of IL-6, u-PA, MUC1; 0.2 ng mL^{-1} $VEGF_{165}$

concentration. Therefore, as presented in Fig. 4 B, a linear relationship between the logarithm of the concentration of $VEGF_{165}$ and the ECL signal was acquired in the range of 2 pg mL^{-1} to 2 ng mL^{-1}, wider than previously reported ranges (shown in Table 1) [37–42]. The regression equation was $I = 1016.1934 \log C_{VEGF165}/\text{pg mL}^{-1} + 2815.6173$, and the correlation coefficient was 0.99645. The detection limit was evaluated to be 0.68 pg mL^{-1} for detecting $VEGF_{165}$, which is lower than previously reported ranges (shown in Table 1) [37–42].

Reproducibility, selectivity, and stability

To estimate the selectivity of the ECL biosensor, the materials interleukin-6 (IL-6), urokinase-type plasminogen activator (u-PA), and mucin 1 (MUC1) were selected for an interference test. As presented in Fig. 4 C, the ECL value of the prepared biosensor for detecting 0.2 ng mL^{-1} $VEGF_{165}$ showed a direct increase compared with the blank test. When 20 ng mL^{-1} concentrations of the interfering materials IL-6, u-PA, and MUC1 were measured by the prepared biosensor, the ECL signals were almost the same as those of the blank test. The ECL intensity of the biosensor incubated with $VEGF_{165}$ (0.2 ng mL^{-1}) containing 20 ng mL^{-1} concentrations of all of the interfering materials was nearly unchanged from the ECL intensity obtained for the biosensor incubated with $VEGF_{165}$ alone. Hence, the results verified that the constructed ECL biosensor had good selectivity for the detection of $VEGF_{165}$. In addition, the reproducibility of the sensor results is vital and plays an important role in analytical methods. The detection results of three electrodes under the same conditions were analyzed to evaluate the reproducibility of the ECL biosensor. The RSD value was 2.74% for 0.2 ng mL^{-1} $VEGF_{165}$, which means that the designed

Table 1 Comparison of analytical performance for $VEGF_{165}$ detection by our method and those reported previously

Method	Linear range (pg mL^{-1})	Detection limit (μmol mL^{-1})	Repeatability (RSD, %)	Refs.
ECL	2–2000	1.68	2.74	This work
Fluorescence	0.5–10	2388 ± 8	8.60	[37]
Fluorescence	5–50	–	–	[38]
Fluorescence polarization	0.32–5	–	3.85	[39]
Electrochemical	15–60	15.000	–	[40]
Electrochemical	1–20	–	–	[41]
Electrophoretic mobility shift assay	10–1000	–	–	[42]

Table 2 The comparison results of clinical serum samples using the proposed and ELISA methods

Serum samples	1	2	3	4	5
ECL biosensor (pg mL^{-1})	108.265	89.536	72.239	78.554	55.283
ELISA (pg mL^{-1})	104.835	94.691	75.189	84.687	58.088
Error value (pg mL^{-1})	3.45	− 5.16	− 2.90	− 6.13	− 2.80
Relative deviation (%)	3.27	− 5.45	− 3.86	− 7.24	− 4.82

sensor had good reproducibility. The target detection stability of the ECL biosensor under storage was also investigated by storing three prepared electrodes for 2 weeks in a refrigerator at 4 °C. The ECL results fluctuated within an acceptable error range when the ECL biosensor was applied to detect the blank. Thus, the results indicated that the prepared ECL biosensor possessed great stability.

Real sample analysis

To prove the practical application performance of the prepared biosensor, both the prepared ECL sensor and an enzyme-linked immunosorbent assay (ELISA) kit were used for the detection of human serum samples. As shown in Table 2, the ELISA results were consistent with the results of the prepared biosensor. Hence, the prepared biosensor could determine the concentration of $VEGF_{165}$ in serum samples.

Conclusion

In this work, an ultrasensitive ECL biosensor based on a g-C_3N_4/PDDA/CdSe nanocomposite was successfully assembled for the detection of $VEGF_{165}$. The proposed ECL biosensor has a wide detection range from 2 pg mL^{-1} to 2 ng mL^{-1} and a low detection limit of 0.68 pg mL^{-1} for $VEGF_{165}$. This ECL biosensor also displays some excellent characteristics, such as sensitivity, stability, reproducibility, and selectivity. We also used the material and the concept of the designed sensor combined with correlative aptamer DNA to detect kanamycin, and the sensor exhibited a good response. Thus, we used the constructed ECL biosensor for the detection of $VEGF_{165}$, and the results showed that the biosensor is a promising platform and that this method potentially has further use in clinical diagnosis.

Acknowledgments This work was supported by the National Natural Science Foundation of China (Grant Nos. 21575001, 21976001), the Natural Science Foundation of Anhui Province (1508085MB37), and the Open fund for Discipline Construction of Institute of Physical Science and Information Technology.

Compliance with ethical standards

Conflict of interest The authors declare that they have no conflict interest.

Ethical approval The protocol of this study was approved by the medical ethics committee of The First Affiliated Hospital of Anhui Medical University. The blood samples (2 mL) of the participants were collected after informed written consent was provided by the subjects.

References

1. Senger DR, Galli SJ, Dvorak AM, Perruzzi C, Harvey VS, Dvorak HF. Tumor cells secrete a vascular permeability factor that promotes accumulation of ascites fluid. Sci. 1983;21:9983–5.
2. Keck PJ, Hauser SD, Krivi GG, Sanzo K, Warren T, Feder J, et al. Vascular permeability factor, an endothelial cell mitogen related to PDGF. Sci. 1989;246:9–12.
3. Ahmetov II, Williams AG, Popov DV, Lyubaeva EV, Hakimullina AM, Fedotovskaya ON, et al. Hum Genet. 2009;12:126–751.
4. Aiello LP, Pierce EA, Foley E, Takagi H, Chen HH, Riddle L, et al. Suppression of retinal neovascularization in vivo by inhibition of vascular endothelial growth factor (VEGF) using soluble VEGF-receptor chimeric proteins. P Natl Acad Sci USA. 1995;92:10457–61.
5. Omar AR. Targeting vascular endothelial growth factor (VEGF) pathway in gastric cancer: preclinical and clinical aspects. Crit Rev Oncol Hematol. 2015;93:18–27.
6. Do DV, Nguyen QD, Vitti R, Berliner AJ, Gibson A, Saroj N, et al. Intravitreal aflibercept injection in diabetic macular edema patients with and without prior anti-vascular endothelial growth factor treatment. OpHth. 2016;123:850–7.
7. Nakahara H, Song J, Sugimoto M, Hagihara K, Kishimoto T, Yoshizaki K, et al. Anti–interleukin-6 receptor antibody therapy reduces vascular endothelial growth factor production in rheumatoid arthritis. Arthritis Rheum. 2003;8:1521–9.
8. Plate KH, Breier G, Weich HA, Risau W. Vascular endothelial growth factor is a potential tumour angiogenesis factor in human gliomas in vivo. Nat. 1992;359:845–8.
9. Slawomir L, Grazyna E B, Ewa G S, Maciej S, The plasma concentration of VEGF, HE4 and CA125 as a new biomarkers panel in different stages and sub-types of epithelial ovarian tumors.
10. Salven P, Orpana A, Joensuu H. Leukocytes and platelets of patients with cancer contain high levels of vascular endothelial growth factor. ACCR. 1995;5:487–91.
11. Carmeliet P, Jain RK. Angiogenesis in cancer and other diseases. Nat. 2000;407:249–57.
12. Detmar M. Evidence for vascular endothelial growth factor (VEGF) as a modifier gene in psoriasis. J Invest Dermatol. 2004;122.

13. Storkebaum E, Lambrechts D, Carmeliet P. VEGF: once regarded as a specific angiogenic factor, now implicated in neuroprotection. BioEssays. 2004;26:943–54.
14. Tsai M, Wang T, Lin Y, Kuo P, Su YH, Huang H. Aryl hydrocarbon receptor agonists upregulate VEGF secretion from bronchial epithelial cells. J Mol Med. 2015;93:1257–69.
15. Li JL, Sun KX, Chen ZP, Shi JF, Zhou DD, Xie GM. A fluorescence biosensor for VEGF detection based on DNA assembly structure switching and isothermal amplification. Biosens Bioelectron. 2017;89:964–9.
16. Iliuk A, Hu LH, Tao A. Aptamer in bioanalytical applications. Anal Chem. 2011;83:4440–52.
17. Liu HY, Xu SM, He ZM, Deng AP, Zhu JJ. Supersandwich cytosensor for selective and ultrasensitive detection of cancer cells using aptamer-DNA concatamer-quantum dots probes. Anal Chem. 2013;85:3385–92.
18. Peng L, Wu CCS, You MX, Han D, Chen Y, Fu T, et al. Engineering and applications of DNA-grafted polymer materials. Chem Sci. 2013;4:1928–38.
19. Yang XJ, Liu X, Liu Z, Pu F, Ren JS, Qu XG. Near-infrared light-triggered, targeted drug delivery to cancer cells by aptamer gated nanovehicles. Adv Mater. 2012;24:2890–5.
20. Zhao J, He XL, Bo B, Liu XJ, Yin YM, Li GX. A signal-on electrochemical aptasensor for simultaneous detection of two tumor markers. Biosens Bioelectron. 2012;34:249–52.
21. Tuerk C, Gold L. Systematic evolution of ligands by exponential enrichment: RNA ligands to bacteriophage T4 DNA polymerase. Sci. 1990;249:505–10.
22. Cho EJ, Lee JW, Ellington AD. Applications of aptamers as sensors. Rev Anal Chem. 2009;2:241–64.
23. Hianik T, Wang J. Electrochemical aptasensors - recent achievements and perspectives. Electroanaly. 2009;21:1223–35.
24. Song SP, Wang LH, Li J, Zhao JL, Fan CH. Aptamer-based biosensors. Anal Chem. 2008;27:108–17.
25. Suzuki Y, Yokoyama K. Development of a fluorescent peptide for the detection of vascular endothelial growth factor (VEGF). Bioconjug Chem. 2009;10:1793–5.
26. Scapini P, Calzetti F, Cassatella MA. On the detection of neutrophil-derived vascular endothelial growth factor VEGF. J Immunol Methods. 1999;232:121–9.
27. Zhou H, Yue H, Zhou YL, Wang L, Fu ZF. A novel disposable immunosensor based on quenching of electrochemiluminescence emission of $Ru(bpy)_3^{2+}$ by amorphous carbon nanoparticles. Sensors Actuators B Chem. 2015;209:744–50.
28. Chen Z, Ma G, Chen ZH, Zhang YG, Zhang Z, Gao JW, et al. Fabrication and photoelectrochemical properties of silicon nanowires/g-C_3N_4 Core/shell arrays. Appl Surf Sci. 2017;396:609–15.
29. Li RY, Zhang Y, Tu WW, Dai ZH. A photoelectrochemical bioanalysis platform for cells monitoring based on dual signal amplification using in situ generation of electron acceptor coupled with heterojunction. ACS. 2017;9:22289–97.
30. Wang HY, Zhang QH, Yin HS, Wang MH, Jiang WJ, Ai SY. A photoelectrochemical immunosensor for methylated RNA detection based on g-C_3N_4/CdS quantum dots heterojunction and Phos-tag-biotin. Biosens Bioelectron. 2017;95:124–30.
31. Zhang H, Li MX, Li CH, Guo ZH, Dong HL, Wu P, et al. G-Quadruplex DNAzyme-based electrochemiluminescence biosensing strategy for $VEGF_{165}$ detection: combination of aptamer–target recognition and T7 exonuclease-assisted cycling signal amplification. Biosens Bioelectron. 2015;74:98–103.
32. Pang XH, Bian HJ, Wang WJ, Liu C, Khan MS, Wang Q, et al. A bio-chemical application of N-GQDs and g-C_3N_4 QDs sensitized TiO_2 nanopillars for the quantitative detection of $pcDNA_3$-HBV. Biosens Bioelectron. 2017;91:456–64.
33. Zhao M, Fan GC, Chen JJ, Shi JJ, Zhu JJ. Highly sensitive and selective photoelectrochemical biosensor for Hg^{2+} detection based on dual signal amplification by exciton energy transfer coupled with sensitization effect. Anal Chem. 2015;87:12340–7.
34. Zhang XR, Li SG, Jin X, Li XM. Aptamer based photoelectrochemical cytosensor with layer-by-layer assembly of CdSe semiconductor nanoparticles as photoelectrochemically active species. Biosens Bioelectron. 2011;26:3674–8.
35. Jie GF, Chen K, Wang XC, Lu ZK. Dual-stabilizer-capped CdSe quantum dots for off-on electrochemiluminescence biosensing of thrombin by target-triggered multiple amplification. RSC Adv. 2016;6:2065–71.
36. Du XL, Kang TF, Lu LP, Cheng SY. An electrochemiluminescence sensor based on CdSe@CdS functionalized MoS_2 and hemin/Gquadruplex-based DNAzyme biocatalytic precipitation for sensitive detection of Pb(II). Anal Methods. 2018:51–8.
37. Kopra K, Syrjanp M, Hanninen P, Harma H. Non-competitive aptamer-based quenching resonance energy transfer assay for homogeneous growth factor quantification. Analyst. 2014;139:2016–23.
38. bMita C, bAbeK, Fukaya T, Ikebukuro K. Vascular endothelial growth factor (VEGF) detection using an aptamer and PNA-based bound/free separation system, Materials. Mater. 2014;7:1046–54.
39. Wang SE, Huang Y, Hu K, Tian JN, Zhao SL. A highly sensitive and selective aptasensor based on fluorescence polarization for the rapid determination of oncoprotein vascular endothelial growth factor (VEGF). Anal Methods. 2014;6:62–6.
40. Nonaka Y, Abe K, Ikebukuro K. Electrochemical detection of vascular endothelial growth factor with aptamer sandwich. Electrochem. 2012;80:363–6.
41. Zhao J, He XL, Bo B, Liu XJ, Yin YM, Li GX. A "signal-on" electrochemical aptasensor for simultaneous detection of two tumor markers. Biosens Bioelectron. 2012;34:249–52.
42. Abe K, Hasegawa H, Ikebukuro K. Electrochemical detection of vascular endothelial growth factor by an aptamer-based bound/free separation system. Electrochem. 2012;80:348–52.
43. Du XL, Lu LP, Cheng SY. An electrochemiluminescence sensor based on CdSe@CdS functionalized MoS2 and hemin/Gquadruplex-based DNAzyme biocatalytic precipitation for sensitive detection of Pb(II). Anal Methods. 2018:10–51.